Journal of Contaminant Hydrology 110 (2009) 87–99

Contents lists available at ScienceDirect

Journal of Contaminant Hydrology

journal homepage: www.elsevier.com/locate/jconhyd

Combined physical and chemical nonequilibrium transport model: Analytical solution, moments, and application to colloids

Feike J. Leij [a], Scott A. Bradford [b,*]

[a] Dept. of Civil Engineering and Construction Engineering Management, California State University, Long Beach, CA, United States
[b] US Salinity Laboratory, USDA, ARS, Riverside, CA, United States

ARTICLE INFO

Article history:
Received 3 March 2009
Received in revised form 7 September 2009
Accepted 11 September 2009
Available online 21 September 2009

Keywords:
Physical nonequilibrium
Chemical nonequilibrium
Preferential flow
Model
Analytical solution
Moments

ABSTRACT

The transport of solutes and colloids in porous media is influenced by a variety of physical and chemical nonequilibrium processes. A combined physical–chemical nonequilibrium (PCNE) model was therefore used to describe general mass transport. The model partitions the pore space into "mobile" and "immobile" flow regions with first-order mass transfer between these two regions (i.e, "physical" nonequilibrium or PNE). Partitioning between the aqueous and solid phases can either proceed as an equilibrium or a first-order process (i.e, "chemical" nonequilibrium or CNE) for both the mobile and immobile regions. An analytical solution for the PCNE model is obtained using iterated Laplace transforms. This solution complements earlier semi-analytical and numerical approaches to model solute transport with the PCNE model. The impact of selected model parameters on solute breakthrough curves is illustrated. As is well known, nonequilibrium results in earlier solute breakthrough with increased tailing. The PCNE model allows greater flexibility to describe this trend; for example, a closer resemblance between solute input and effluent pulse. Expressions for moments and transfer functions are presented to facilitate the analytical use of the PCNE model. Contours of mean breakthrough time, variance, and spread of the colloid breakthrough curves as a function of PNE and CNE parameters demonstrate the utility of a model that accounts for both physical and chemical nonequilibrium processes. The model is applied to describe representative colloid breakthrough curves in Ottawa sands reported by Bradford et al. (2002). An equilibrium model provided a good description of breakthrough curves for the bromide tracer but could not adequately describe the colloid data. A considerably better description was provide by the simple CNE model but the best description, especially for the larger 3.2-μm colloids, was provided by the PCNE model.

Published by Elsevier B.V.

1. Introduction

The transport of solutes and colloids in porous media is subject to a variety of nonequilibrium processes. Physical nonequilibrium (PNE) will affect transport because of nonuniformity of the flow field at the pore scale including preferential and unstable flow (Ritsema et al., 1993; de Rooij, 2000; Wang et al., 2004). The mobile/immobile model has commonly been used to account for PNE during solute transport (Coats and Smith, 1964; van Genuchten and Wierenga, 1976). In this case, the pore space is partitioned into two regions. Transport in the "mobile" region of the pore space is described with the advection–dispersion equation (ADE) while solute exchange between "mobile" and "immobile" regions occurs by diffusion and is typically described with a first-order rate equation. The mobile/immobile model predicts early initial breakthrough as a result of rapid transport through the "mobile" region, and extended tailing of the breakthrough curve as a result of slow diffusion between the "immobile" to the "mobile" region.

Chemical nonequilibrium (CNE) occurs as a result of rate-limited chemical reactions at an interface (Sparks, 198). Reduced mass transfer rates of solutes to/from an interface

* Corresponding author. Tel.: +1 951 369 4857.
E-mail address: sbradford@ussl.ars.usda.gov (S.A. Bradford).

0169-7722/$ – see front matter. Published by Elsevier B.V.
doi:10.1016/j.jconhyd.2009.09.004

are manifested in delayed interactions between solute and interface and may also be modeled as a PNE process. CNE models have been used for several decades to elucidate and quantify solute transport in porous media (Coats and Smith, 1964; Selim and Ma, 1998). CNE models are typically based on the ADE with linear driving force terms to describe rate-limited mass transfer and reaction behavior (Powers et al., 1991). Linear driving force models are quasi-steady state approximations of Fick's first law of diffusion and assume that the rate of mass transfer is equal to the product of the diffusional resistance in and the concentration difference across the boundary layer. In contrast to PNE models, CNE models only affect the concentration of solutes and/or colloids that interact with an interface. The mathematical solution for both models is essentially the same (Toride et al., 1993). However, it is desirable to have a model that accounts for both the conceptually different PNE and CNE processes because physical and chemical nonequilibrium will affect transport differently than simple PNE or CNE (cf. Wagenet and Chen, 1998). The combined physical and chemical nonequilibrium (PCNE) model provides the flexibility to independently describe physical and chemical nonequilibrium effects.

Brusseau et al. (1989) considered the multiprocess nonequilibrium transport of solutes subject to rate-limited mass transfer in the liquid and the sorbent. The model was extended to include first-order degradation by Brusseau et al. (1992). Selim et al. (1999) used both a two-site CNE model, with either equilibrium or kinetic sorption, and PNE to describe pesticide transport in soil. The solute or pesticide concentrations were obtained numerically. Analytical solutions can typically only be obtained for linear transport problems for simplified conditions. This limits their applicability to well-defined conditions such as those in laboratory experiments. However analytical methods are also useful to verify numerical methods, elucidate the role of different model parameters, and to approximately quantify transport such as for longer time or spatial scales. It should also be noted that detailed numerical simulations are often not warranted because of a lack of reliable model parameters. Therefore analytical results for the PCNE model will still be valuable. Neville et al. (2000) proposed a semi-analytical approach. After applying a Laplace transform of the governing equations for the PCNE model, the solute concentration was obtained by numerical inversion. The major objective of this work is to derive analytical tools for the PCNE model that offer the flexibility to independently quantify the impact of a "chemical" and "physical" nonequilibrium process on solute transport.

Solute transport models such as the CNE model have frequently been used to describe the movement of colloids in porous media since the attachment and detachment of colloids on the solid phase is not an equilibrium process. However, colloids are subject to additional nonequilibrium due to differences in flow and pore geometry that is typically described with a PNE model (Leij and Toride, 1998). Simulations of the flow field between the solid grains of a porous medium clearly show eddy zones that are hydrodynamically isolated from the bulk fluid flow (Torkzaban et al., 2008). Any transfer of colloids into and from these regions will be diffusion controlled. Colloid transport and retention in porous media with such "immobile" zones are more complicated than for "conventional" solutes such as inorganic electrolytes. Colloids that are weakly associated with solid-water and/or air-water interfaces can be funneled by hydrodynamic forces to immobile regions under unfavorable attachment conditions (Johnson et al., 2007; Torkzaban et al., 2008). Colloid retention is inversely related to pore-water velocity (Bradford and Torkzaban, 2008; Torkzaban et al., 2008) and is also affected by the pore-size distribution, the colloid size, and the water content (Bradford et al., 2006, 2007; Torkzaban et al., 2008). Applied and resisting torque balance calculations indicate that the volume of the pore space where colloid retention may occur will decrease with increasing fluid velocity and decreasing adhesive forces (Torkzaban et al., 2007). The PCNE model appears particularly suited to describe colloid transport to permit (different) rate equations for colloid attachment and detachment (CNE) with the magnitude of the difference depending on the flow regime (PNE). A secondary objective of this work is to apply the new solution of the PCNE model to describe colloid breakthrough curves reported by Bradford et al. (2002).

2. Theoretical

2.1. Problem formulation

The two governing equations for transport of a solute in a porous medium (soil) with mobile and immobile regions of soil water are defined as:

$$\theta_m \frac{\partial C_m}{\partial t} + \theta_{im} \frac{\partial C_{im}}{\partial t} + \rho_b \frac{\partial S}{\partial t} = \theta_m D_m \frac{\partial^2 C_m}{\partial z^2} - \theta_m v_m \frac{\partial C_m}{\partial z} \quad (1)$$

$$\theta_{im} \frac{\partial C_{im}}{\partial t} + \rho_b \frac{\partial S_{im}}{\partial t} = \alpha (C_m - C_{im}) \quad (2)$$

where θ is the volumetric water content, the subscripts m and im refer to the mobile and immobile region, C is solute concentration in the aqueous phase [M/L^3], S is the solid phase concentration of solute from either the mobile or immobile region per mass of dry soil [M/M], ρ_b is the dry soil bulk density [M/L^3], D is the dispersion coefficient [L^2/T], v is the pore-water velocity [L/T], α is a PNE coefficient for mass transfer between mobile and immobile region [1/T], z is depth [L], and t is time [T]. When colloids are considered the aqueous and solid phase concentrations are typically given in terms of number, rather than the mass.

The aqueous phase consists of mobile and immobile regions. The solid phase of the soil is either in contact with the mobile or immobile aqueous region, solutes may sorb onto or desorb from the solid phase. Without considering the actual mechanism for solute sorption, the following equalities hold:

$$\theta_m + \theta_{im} = \theta\,, \quad \theta_m v_m = \theta_v\,, \quad \theta_m D_m = \theta D\,, \quad S_m + S_{im} = S. \quad (3a,b,c,d)$$

The CNE component is introduced by further distinguishing between equilibrium (type 1) and kinetic (type 2) retention:

$$S_m = S_{m,1} + S_{m,2}\,, \quad S_{im} = S_{im,1} + S_{im,2}. \quad (4a,b)$$

Fig. 1 illustrates the different concentration types that may occur. The relationship between concentrations may be quantified with transfer functions H as discussed later on. Notice that nonequilibrium retention is depicted different in Fig. 1 than the corresponding nonequilibrium exchange for solutes by Brusseau et al. (1989). These authors, among others, consider intrasorbent diffusion rather than rate-limited sorption as the reason for nonequilibrium transport. However, the mathematical problem for nonequilibrium solute sorption will be the same for either kinetic exchange, intrasorbent diffusion, or both these processes because C_m and S_{m1} are linearly dependent. Solute sorption on type-1 sites is an equilibrium process described by:

$$S_{m,1} = K_{m,1}C_m \ , \quad S_{im,1} = K_{im,1}C_{im} \tag{5a, b}$$

with K as a "distribution" constant expressed as volume of aqueous phase (either the "mobile" or "immobile" region) per mass of dry soil [L^3/M]. Sorption on type-2 sites is governed by a first-order rate equation:

$$\frac{\partial S_{m,2}}{\partial t} = \beta_m(K_{m,2}C_m - S_{m,2}) \ , \quad \frac{\partial S_{im,2}}{\partial t} = \beta_{im}(K_{im,2}C_{im} - S_{im,2}). \tag{6a, b}$$

The sorption rate is proportional to the difference in (eventual) equilibrium and actual solid phase concentration with β as the proportionality constant [1/T]. These coefficients are likely to be different for retention from the mobile and immobile regions. For both regions a ratio of "equilibrium" to "total" sites may be defined. At equilibrium these follow from the solid phase concentrations or the distribution coefficients according to:

$$f_m = \frac{S_{m,1}}{S_m} = \frac{K_{m,1}}{K_m} \ , \quad f_{im} = \frac{S_{im,1}}{S_{im}} = \frac{K_{im,1}}{K_{im}}. \tag{7a, b}$$

The equilibrium concentrations are shown on the left-hand side of Fig. 1. The total concentration, which is given as mass per volume of bulk soil, is defined as:

$$C_T = \theta_m C_m + \theta_{im} C_{im} + \rho_b(S_m + S_{im}). \tag{8}$$

At equilibrium, the total concentration is given by:

$$C_T = \theta R C_m \ \text{with} \ R = 1 + \rho_b K / \theta \ \text{and} \ K = K_m + K_{im} \tag{9}$$

where R is a retardation factor (cf. Table 1).

The system of mathematical equations that needs to be solved is as follows:

$$\theta_m \frac{\partial C_m}{\partial t} + \theta_{im} \frac{\partial C_{im}}{\partial t} + \rho_b \left(f_m K_m \frac{\partial C_m}{\partial t} + \frac{\partial S_{m,2}}{\partial t} + f_{im} K_{im} \frac{\partial C_{im}}{\partial t} + \frac{\partial S_{im,2}}{\partial t} \right) = \theta_m D_m \frac{\partial^2 C_m}{\partial z^2} - \theta_m v_m \frac{\partial C_m}{\partial z} \tag{10a}$$

$$\theta_{im} \frac{\partial C_{im}}{\partial t} + \rho_b \frac{\partial S_{im}}{\partial t} = \alpha(C_m - C_{im}) \tag{10b}$$

$$\frac{\partial S_{m,2}}{\partial t} = \beta_m[(1-f_m)K_m C_m - S_{m,2}] \ , \quad \frac{\partial S_{im,2}}{\partial t} = \beta_{im}[(1-f_{im})K_{im} C_{im} - S_{im,2}]. \tag{10c, d}$$

The problem will be rewritten with C_m as a dependent variable because the other concentration types as well as influent and effluent concentrations are most easily expressed in terms of C_m. The selected mathematical conditions involve a zero initial condition and a time-dependent input $C_o(t)$:

$$C_m(z, 0) = 0 \tag{11}$$

$$C_m(0, t) = C_o(t) \ , \ C_m(\infty, t) = 0. \tag{12a, b}$$

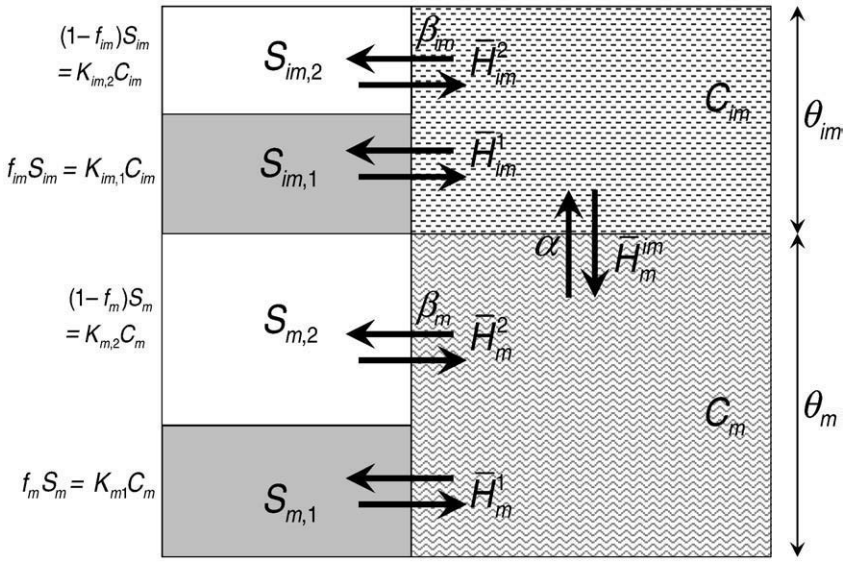

Fig. 1. Schematic of different concentration types for physical–chemical nonequilibrium transport model.

Table 1
Parameters for PNE, CNE, and PCNE models.

Model	Auxiliary parameters			
PNE	$a_m = \frac{\alpha}{\theta_m R_m}$		$a_{im} = \frac{\alpha}{\theta_{im} R_{im}}$	
CNE		$b_m = \frac{\beta R_2}{R_1}$		
PCNE	$a_m = \frac{\alpha}{\theta_m R_{m,1}}$	$b_m = \frac{\beta_m R_{m,2}}{R_{m,1}}$	$a_{im} = \frac{\alpha}{\theta_{im} R_{im,1}}$	$b_{im} = \frac{\beta_{im} R_{im,2}}{R_{im,1}}$
	Retardation factors			
PNE	$R_m = 1 + \rho_b K_m/\theta_m$		$R_{im} = 1 + \rho_b K_{im}/\theta_{im}$	
CNE	$R_1 = 1 + \rho_b f K/\theta$		$R_2 = \rho_b(1-f)K/\theta$	
PCNE	$R_{m,1} = 1 + \rho_b f_m K_m/\theta_m$		$R_{im,1} = 1 + \rho_b f_{im} K_{im}/\theta_{im}$	
	$R_{m,2} = \rho_b(1-f_m)K_m/\theta_m$		$R_{im,2} = \rho_b(1-f_{im})K_{im}/\theta_{im}$	
	$R_m = 1 + \rho_b K_m/\theta_m$		$R_{im} = 1 + \rho_b K_{im}/\theta_{im}$	
All	$R = 1 + \rho_b K/\theta$			

2.2. Solution of the PCNE

The solution of the mobile concentration for the physical–chemical nonequilibrium (PCNE) model is outlined in Appendix A. The mobile concentration for an arbitrary input $C_o(t)$ is:

$$C_m(z,t) = \int_0^t C_o(t-\tau)\left\{h(z,\tau,0) + \int_0^\tau h(z,\tau,\eta)\left[f(\tau,\eta,\eta,0) + g_m(\tau,\eta,0) + \int_0^\eta g_{im}(\eta,\sigma,0)f(\tau,\eta,\eta,\sigma) + g_m(\tau,\eta,\sigma)\left(f(t,\eta,\sigma,0) + \int_0^\sigma g_{im}(\sigma,\kappa,0)f(\tau,\eta,\sigma,\kappa)d\kappa\right)d\sigma\right]d\eta\right\}d\tau \quad (13)$$

where τ, η, σ, and κ are dummy integration variables. The auxiliary functions f, g, and h are defined as follows:

$$f(\tau,\eta,\sigma,\kappa) = \sqrt{\frac{a_m a_{im}(\tau-\eta)}{\sigma-\kappa}}\, exp\left[-(a_{im} + b_{im})(\sigma-\kappa)\right] \times I_1\left[\sqrt{4a_m a_{im}(\tau-\eta)(\sigma-\kappa)}\right] \quad (14a)$$

$$g_j(\eta,\sigma,\kappa) = \sqrt{\frac{\beta_j b_j(\eta-\sigma)}{\sigma-\kappa}}\, exp\left[-\beta_j(\sigma-\kappa)\right] \times I_1\left[\sqrt{4\beta_j b_j(\eta-\sigma)(\sigma-\kappa)}\right] (j = m, im) \quad (14b)$$

$$h(z,\tau,\eta) = \frac{z}{\sqrt{4\pi D_m(t-\tau)^3/R_{m,1}}} \times exp\left(-(a_m + b_m)(\tau-\eta) - \frac{\left[R_{m,1}z - v_m(\tau-\eta)\right]^2}{4D_m R_{m,1}(\tau-\eta)}\right) \quad (14c)$$

with I_1 as the first-order modified Bessel function. The auxiliary parameters a_j and b_j are defined in Table 1. Note that Table 1 also provides results for the limiting cases of PCE and CNE.

The expressions for the immobile concentration C_{im} and the different types of concentrations for the solid phase ($S_{m,1}$, $S_{m,2}$, $S_{im,1}$, and $S_{im,2}$) follow from these results as outlined in Appendix B. Special cases of the problem arise when $\beta_m = \beta_{im} = 0$ (i.e., exclusive physical nonequilibrium PNE) and $\alpha = 0$ (i.e., chemical nonequilibrium CNE). The additional nonequilibrium process that is included in the PCNE complicates the mathematical problem; existing solutions for the PNE or CNE models such as derived by Toride et al. (1993) cannot be readily adapted.

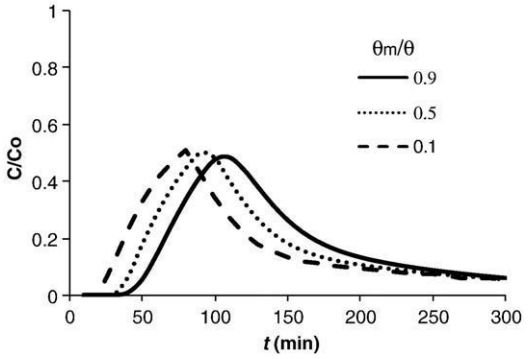

Fig. 2. Normalized concentration as a function of time according to the PCNE model for a 10-cm long soil column with $t_o = 60$ min, $q = \theta_m v_m = 0.25$ cm/min, $D_m = 0.05$ cm^2/min, $\rho_b = 1.325$ g/cm^3, $\theta = 0.5$, $\alpha = 0.01$ min^{-1}, $\beta_m = \beta_{im} = 0.1$ min^{-1}, $f_m = f_{im} = 0.5$, $K_m = 0.4$ cm^3 g^{-1}, and $K_{im} = 0.6$ cm^3 g^{-1} for three values of θ_m/θ.

2.3. Applications

The solution for the PCNE is now used to illustrate the sensitivity of the breakthrough curve to different types of nonequilibrium. Values for the model parameters are adapted from Leij and Toride (1998) and Bradford et al. (2002), but the solution can obviously be applied to different sets of parameters. Fig. 2 shows effluent breakthrough curves as a function of actual time when physical nonequilibrium ($\alpha = 0.01$ min^{-1}) is more pronounced than chemical nonequilibrium ($\beta_m = \beta_{im} = 0.1$ min^{-1}) for three mobile water fractions ($\theta_m = 0.05$, 0.25, and 0.45) and the same Darcy velocity $q = \theta_m v_m = 0.25$ cm/min. There is slightly earlier breakthrough and more tailing for the lower θ_m/θ but the shapes of the curves are similar. Now consider a scenario with both physical ($\alpha = 0.01$ min^{-1}) and chemical ($\beta_m = \beta_{im} = 0.01$ min^{-1}) nonequilibrium where the fraction of solid phase ("sites") with equilibrium that partitions with the aqueous phase varies (Fig. 3). If most of the partitioning is a nonequilibrium process ($f_m = f_{im} = 0.1$), the solute appears

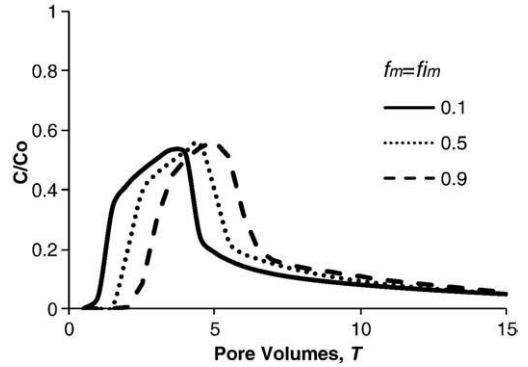

Fig. 3. Breakthrough curves according to the PCNE model for a 10-cm long soil column with $t_o = 60$ min, $v_m = 0.5$ cm/min, $D_m = 0.05$ cm^2/min, $\rho_b = 1.325$ g/cm^3, $\theta_m = \theta_{im} = 0.25$ with $\theta = 0.5$, $\alpha = 0.01$ min^{-1}, $\beta_m = \beta_{im} = 0.01$ min^{-1}, $K_m = 0.4$ cm^3 g^{-1}, and $K_{im} = 0.6$ cm^3 g^{-1} for $f_m = f_{im}$ equal to either 0.1, 0.5, or 0.9.

somewhat earlier in the effluent and there will be slightly more tailing. However, the general shape of the breakthrough curve does not alter much if exchange between solid and aqueous becomes more of an equilibrium process (i.e., f increases to 0.5 or 0.9).

Of particular interest for studying the combined effect of physical and chemical nonequilibrium parameters is the dependency of the breakthrough curve on both rate parameters α and β. Fig. 4 displays breakthrough curves for physical rate parameter α equal to 0.1, 0.01, or 0.001 min^{-1} and the chemical nonequilibrium parameter β, also equal to 0.1, 0.01, or 0.001 min^{-1}. The latter values are based upon the detachment rates reported by Bradford et al. (2002) assuming that $\beta_m = \beta_{im}$. A decrease in exchange between mobile and immobile regions of the aqueous phase (i.e., lower values for α) results in earlier breakthrough and a higher peak concentration. The longer tail is not shown in Fig. 4. The behavior is similar as for the PNE model (Leij and Toride, 1998). Due to chemical nonequilibrium, the breakthrough curve exhibits a higher maximum concentration and steeper gradients (i.e., a more rectangular curve) for lower β. During nonequilibrium conditions, assuming unchanged θ_m, K_m, and K_{im}, solutes are less likely to move from the aqueous to the solid phase (CNE) or from mobile into the immobile aqueous phase (PNE). If they do, the reverse transfer back into the mobile aqueous phase and the subsequent appearance in the effluent will also proceed more slowly. Hence, chemical nonequilibrium enhances the differentiation between solute travel times with a greater amount of solute appearing early in the effluent as a more rectangular part of the breakthrough curve, the remaining solute will reside longer in the porous medium. The chemical nonequilibrium component of the PCNE allows more flexibility to simulate the residence times of solutes without impacting the pore-water velocity (which is determined by the Darcy flux and θ_m).

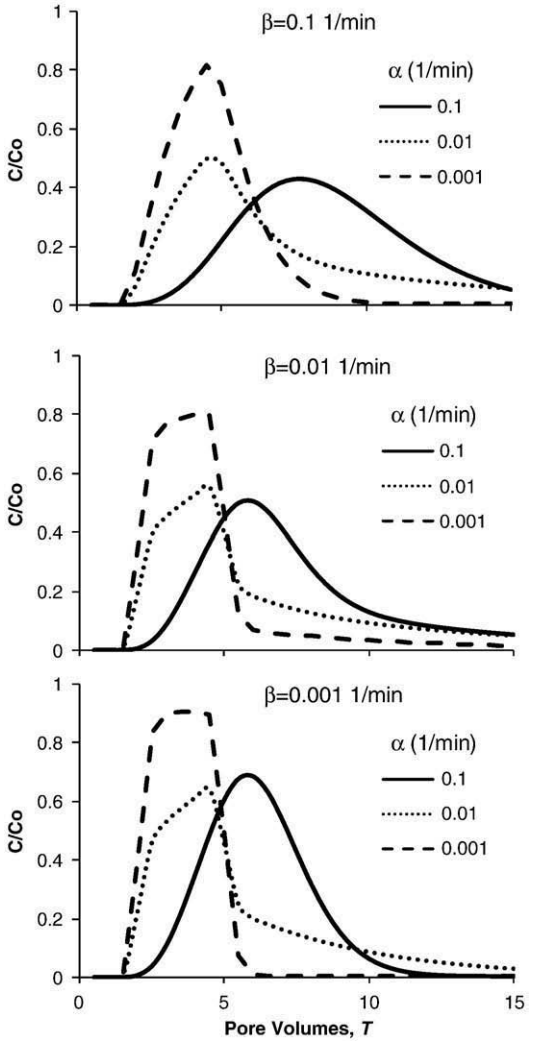

Fig. 4. Breakthrough curves according to the PCNE model for a 10-cm long soil column with $t_o = 60$ min, $v_m = 0.50$ cm/min, $D_m = 0.05$ cm^2/min, $\rho_b = 1.325$ g/cm^3, $\theta_m = \theta_{im} = 0.25$, $f_m = f_{im} = 0.5$, $K_m = 0.4$ $\text{cm}^3\,\text{g}^{-1}$, and $K_{im} = 0.6$ $\text{cm}^3\,\text{g}^{-1}$ for three values of α and $\beta_m = \beta_{im} = \beta$.

With the analytical solution, additional sensitivity analyses involving aqueous or solid concentration profiles versus time or distance may be performed for one or more PCNE parameters (v_m, D_m, K_m, K_{im}, θ_m, α, β_m, β_{im}, f_m, f_{im}). Furthermore, the PCNE model can be readily simplified by setting parameters to zero or reformulated by regrouping parameters. For example, for colloid transport it is common to use different attachment and detachment rates and to assume that all partitioning should be described as a nonequilibrium process (cf. Bradford et al., 2002). Partitioning between the mobile or immobile aqueous and the solid phase may be written as:

$$\frac{\partial S_m}{\partial t} = \frac{\theta_m k_{m,a}}{\rho_b} C_m - k_{m,d} S_m \,, \quad \frac{\partial S_{im}}{\partial t} = \frac{\theta_{im} k_{im,a}}{\rho_b} C_{im} - k_{im,d} S_{im} \tag{15a, b}$$

where $k_{m,a}$ and $k_{m,d}$ are rate coefficients [T^{-1}] for attachment (retention) and detachment (release) of colloids from the mobile region, $k_{im,a}$ and $k_{im,d}$ are the corresponding coefficients [T^{-1}] for the immobile region. They can be related to the parameters in the general PCNE model according to:

$$\beta_m = k_{m,d}, \quad K_m = \frac{\theta_m k_{m,a}}{\rho_b k_{m,d}} \,, \quad \beta_{im} = k_{im,d}, \quad K_{im} = \frac{\theta_{im} k_{im,a}}{\rho_b k_{im,d}}. \tag{16a, b, c, d}$$

2.4. Transfer functions and moments

The different types of aqueous and solid phase concentrations can be conveniently related with each other using transfer functions (Sardin et al., 1991). These functions are in essence the ratio of an "output" to an "input" signal in the Laplace or frequency domain. Fig. 1 depicts functions for the PCNE with transfer between the different aqueous and solid phases. Transfer from the mobile to the immobile region is governed by:

$$\overline{H}_m^{\,im}(p) = \frac{\overline{C}_{im}(p,z)}{\overline{C}_m(p,z)} = \frac{a_{im}(p + \beta_{im})}{(p + a_{im} + b_{im})(p + \beta_{im}) - \beta_{im} b_{im}} \tag{17}$$

Table 2
Expressions for first-, second-, and third-order moments for breakthrough after a Dirac delta input according to PNE, CNE, and PCNE models.

Model	M_1	M_2	M_3
PNE	$\frac{Rz}{v}$	$z\left[\frac{R^2}{v^3}(2D+vz)+\frac{2\theta_{im}^2R_{im}^2}{\alpha\theta v}\right]$	$z\left[\frac{R^3}{v^5}(12D^2+6Dvz+v^2z^2)+\frac{6\theta_{im}^2R_{im}^2}{\alpha\theta v}\left(\frac{R}{v^2}(2D+vz)+\frac{\theta_{im}R_{im}}{\alpha}\right)\right]$
CNE	$\frac{Rz}{v}$	$z\left[\frac{R^2}{v^3}(2D+vz)+\frac{2R_2}{\beta v}\right]$	$z\left[\frac{R^3}{v^5}(12D^2+6Dvz+v^2z^2)+\frac{6R_2}{\beta v}\left(\frac{R}{v^2}(2D+vz)+\frac{1}{\beta}\right)\right]$
PCNE	$\frac{Rz}{v}$	$z\left\{\frac{R^2}{v^3}(2D+vz)+\frac{2}{\theta v}\left[\frac{\theta_{im}^2R_{im}^2}{\alpha}+\frac{\theta_{im}R_{im,2}}{\beta_{im}}+\frac{\theta_mR_{m,2}}{\beta_m}\right]\right\}$	$z\left\{\frac{R^3}{v^5}(12D^2+6Dvz+v^2z^2)+\frac{6}{\theta v}\left[\frac{\theta_{im}^2R_{im}^2}{\alpha}\left(\frac{R}{v^2}(2D+vz)+\frac{\theta_{im}R_{im}}{\alpha}\right)+\frac{\theta_{im}R_{im2}}{\beta_{im}}\left(\frac{R}{v^2}(2D+vz)+\frac{1}{\beta_{im}}+\frac{2\theta_{im}R_{im}}{\alpha}\right)+\frac{\theta_mR_{m,2}}{\beta_m}\left(\frac{R}{v^2}(2D+vz)+\frac{1}{\beta_m}\right)\right]\right.$

where the overbar denotes Laplace transformation and p is the Laplace variable (cf. Appendix A). Inversion of the transfer function to the time domain yields:

$$H_m^{im}(t)=\frac{a_{im}}{2w_3}\{(w_1+w_2)exp[-(w_2+w_3)t/2]-(w_1-w_3)exp[-(w_2-w_3)t/2]\} \quad (18a)$$

$$\text{with } w_1=a_{im}+b_{im}-\beta_{im}, \quad w_2=a_{im}+b_{im}+\beta_{im}, \quad w_3=\sqrt{w_2^2-4a_{im}\beta_{im}}. \quad (18b,c,d)$$

This inverse is referred to as the residence time distribution, RTD, which is a probability density function of times required for transfer from the mobile to immobile region. The concentration in the immobile region is a convolution of the mobile concentration and the RTD, i.e.,

$$C_{im}(z,t)=\int_0^\infty H_m^{im}(t-\tau)C_m(z,\tau)d\tau \quad (19)$$

The RTDs for transfer from the mobile and immobile pore space into the corresponding solid phases are respectively given by:

$$H_m^1(t)=\delta(t)K_{m,1}\ ,\ H_m^2(t)=K_{m,2}\beta_m exp(-\beta_m t) \quad (20a,b)$$

$$H_{im}^1(t)=\delta(t)K_{im,1}\ ,\ H_{im}^2(t)=K_{im,2}\beta_{im}exp(-\beta_{im}t). \quad (21a,b)$$

Equilibrium partitioning occurs instantaneously and, in this trivial case, the RTD is a Dirac delta function. The transfer function concept is convenient to deal with "in series" transport of solutes from the mobile via the immobile to the type 2 solid phase, or the "parallel" process of sorption by sites with different rate coefficients.

Evaluation of the analytical expressions for the concentration according to the PCNE is cumbersome in view of the integrations. Instead, solute breakthrough may be more conveniently characterized with the following time moments:

$$m_n(z)=\int_0^\infty t^nC(z,t)dt\ (n=0,1,2\ldots) \quad (22)$$

where n is the order of the moment and C is the dependent variable. As is well known, moments can be conveniently obtained from the solution in the temporal Laplace domain according to:

$$m_n(z)=\lim_{p\to0}\frac{d^n\,\overline{C}}{dp^n}\ ,\ M_n(z)=\frac{m_n(z)}{m_0(z)} \quad (23a,b)$$

with p as the Laplace variable and M as the normalized moment.

The solution in the Laplace domain is given in Appendix A (i.e., Eq. (A9)). With the help of mathematical software, expressions for the first three moments were derived for the PNE, CNE, and PCNE models for a Dirac-type input of a unit mass (i.e., $m_0=1$). Table 2 shows the results. From these expressions follow the mean breakthrough time, $\mu=M_1$, the variance about the mean, $\sigma^2=M_2-(M_1)^2$, and the skewness, $\gamma=M_3/\sigma^3$. Mean breakthrough time is not affected by nonequilibrium parameters for the PCNE model, as was already observed for PNE and CNE (Valocchi, 1985; Leij and Toride, 1998). The second moment quantifies solute dispersion, which depends on nonequilibrium processes but physical and chemical nonequilibrium phenomena act independently. The skewness of the breakthrough curve for the PCNE model will be larger than predicted according to mere physical or chemical nonequilibrium due to the "cross" term.

The moment results were used to examine the sensitivity of colloid displacement to transport parameters. For brevity, the sensitivity will be considered for two parameters at a time. Consider the transfer between mobile and immobile regions and subsequent colloid retention. Fig. 5 depicts contours for mean breakthrough time M_1 (min), variance (min^2), and skew as a function of logα and log$k_{im,a}$ for a breakthrough curve at $z=10$ cm. As is well known (Sardin et al., 1991), the mean breakthrough time M_1 is not affected by the transfer coefficient α, but it does depend on the amount of colloids that will be retained and hence on $k_{im,a}$. The variance (dispersion) of the breakthrough increases with α up to log $\alpha=-2$ and increases throughout with log $k_{im,a}$. The skewness changes rapidly for log$\alpha<-2$ and log$k_{im,a}>-2$ and exhibits a more gradual change elsewhere. In the other use of moments, Fig. 6 shows the dependency of mean breakthrough time, variance and skew on immobile water content θ_{im} and, again, deposition rate $k_{im,a}$. Larger values for M_1, Var, and γ tend to occur for larger θ_{im} and $k_{im,a}$, which both imply increased colloid retention. The mean breakthrough time appears to depend more strongly on $k_{im,a}$ whereas skewness is mostly determined by θ_{im}.

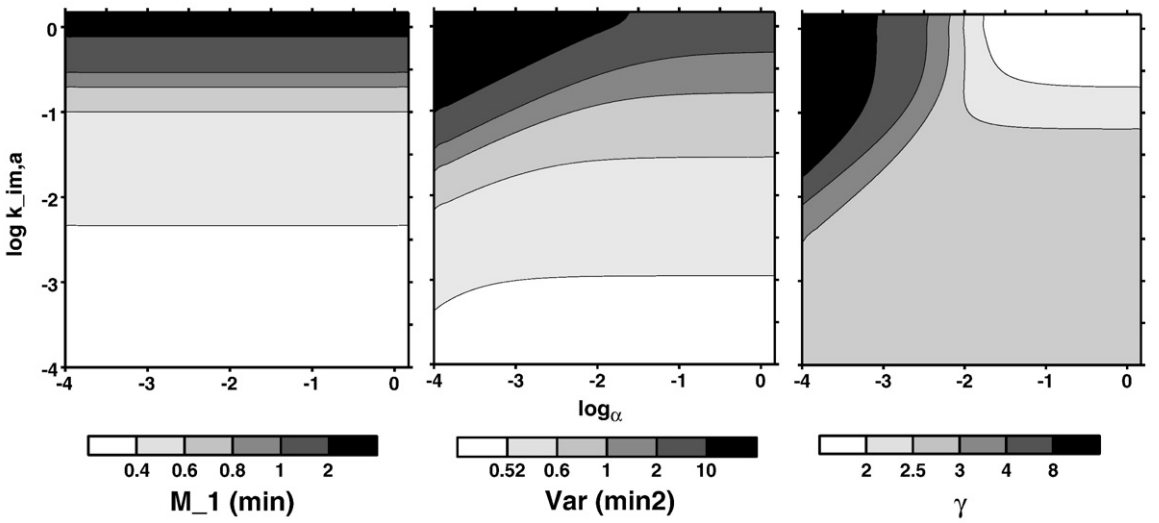

Fig. 5. Contours for mean breakthrough time (M_1, min), variance (Var, min^2), and skew (γ) as a function of logα (with mass transfer coefficient α in min^{-1}) and log $k_{im,a}$ (with $k_{im,a}$ also in min^{-1}) for instantaneous colloid application and $z=10$ cm with $v_m=0.339$ cm/min, $D_m=0.0339$ cm^2/min, $\theta_m=0.301$, $\theta_{im}=0.0334$, $\rho_b=1.76$ g/cm^3, $f_m=f_{im}=0$, $k_{m,a}=0.0201$ min^{-1}, $k_{m,d}=0.001$ min^{-1}, and $k_{im,d}=0.001$ min^{-1}.

3. Colloid transport

The analytical results can be used to quantify and elucidate a wide variety of transport scenarios involving breakthrough curves and retention profiles. In this study the solutions were applied to describe colloid breakthrough curves reported by Bradford et al. (2002). During a steady flow of buffered aqueous solutions with a Darcy velocity of approximately 0.1 cm min^{-1}, a pulse with carboxyl latex microspheres and a bromide tracer (0.001 *M* NaBr buffered to a pH of 7) was applied to columns packed with different porous media. Results of four experiments were used (Table 3). The porous medium consists of Ottawa quartz sand with a median grain diameter of either 710 μm (denoted as "2030") or 240 μm (denoted as "mix"). For both media the colloid diameter was either 0.45 or 3.2 μm. The latter is typical for the size of pathogenic bacteria. The corresponding colloid concentrations in the pulse solution are approximately 4.24×10^{11} and 1.18×10^{9} particles/L yielding a total mass of applied colloids of approximately 3.28 mg. Table 3 lists the Darcy flux (q), column length (L), and porosity (ε) for the column experiments. The reader is referred to Bradford et al. (2002) for more extensive details.

First consider the breakthrough curves for the bromide tracer with results listed below the experimental conditions in Table 3. Moments of the breakthrough curve, concentration

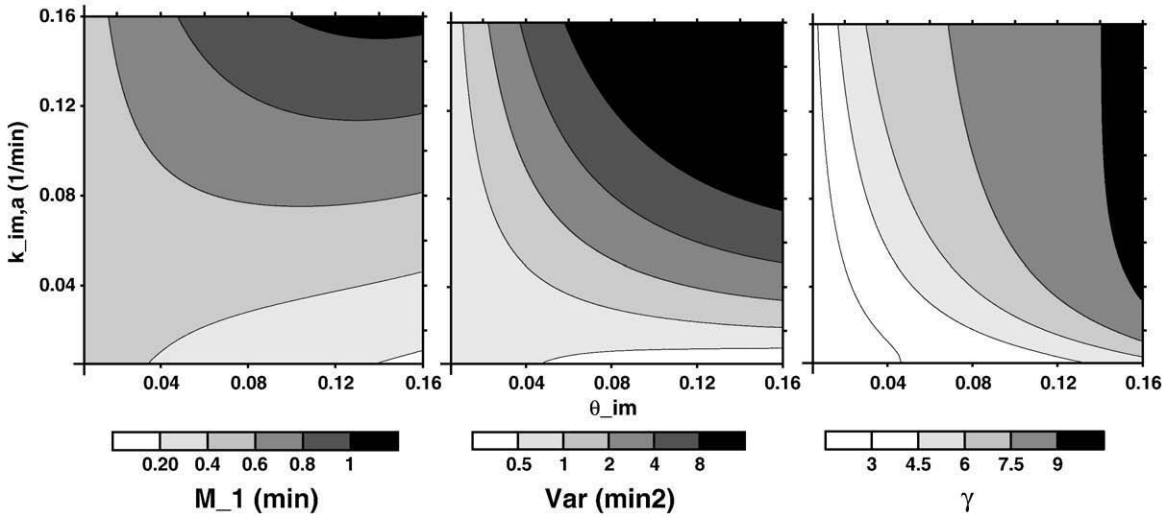

Fig. 6. Contours for mean breakthrough time (M_1, min), variance (Var, min^2), and skew (γ) as a function of immobile water content θ_{im} and rate of attachment from the immobile phase $k_{im,a}$ for instantaneous colloid application and $z=10$ cm with $v_m=0.339$ cm/min, $D_m=0.0339$ cm^2/min, $\alpha=0.001$ min^{-1}, $\theta=0.334$, $\rho_b=1.76$ g/cm^3, $f_m=f_{im}=0$, $k_{m,a}=0.0201$ min^{-1}, $k_{m,d}=0.001$ min^{-1}, and $k_{im,d}=0.001$ min^{-1}.

versus time, were determined according to Eq. (22). The zero-order moment, m_0, yields a value in the order of 70 min. This value was used as the pulse duration t_o in the analysis of the colloid data. The retardation factor for the conventional advection–dispersion equation (ADE) is calculated according to $R=M_1-t_o/2$. Values for R are close to unity as would be expected for a conservative tracer. Higher-order moments will not be presented because these become more inaccurate as the order increases. The breakthrough curves were optimized with the solutions of the ADE and the PNE using the Levenberg–Marquardt procedure. For the ADE, R and D are given in Table 3. The values for the coefficient of determination r^2, suggest a good description of the data. Using the analytical solution for the PNE, which involves the additional nonequilibrium parameters α and the fraction of mobile water θ_m/θ, does not greatly improve the description of the data judging by the r^2 value. The value for θ_m/θ, with θ equal to the porosity ε, is typically close to unity. Equilibrium conditions appear to exist for bromide transport and, as already pointed out by Bradford et al. (2002), bromide serves as a good conservative tracer.

Colloid breakthrough curves are reported as normalized concentration C/C_o, i.e., the ratio of the number of colloid particles in the effluent and the pulse solutions, versus normalized time $T=v_m t/L$. Fig. 7 shows the observations as well as optimized curves for the four experiments. The bottom half of Table 3 contains the experimental moments followed by the optimized parameters for the ADE, PNE, and PCNE models. The breakthrough curves obtained from these fitted parameters are also shown in Fig. 7. Colloid size has a strong negative correlation with the total amount of colloid in the effluent. The values for the zero-order moment m_0 are close to the pulse duration t_o for the smaller 0.45-μm colloids (experiments 1 and 3), but for the larger 3.2-μm colloids only about 45% (experiment 2) and 12% (experiment 4) of the applied colloids end up in the effluent. The finer medium, i.e., a mixture of sand with a median diameter of 240 μm, will retain more colloids (experiment 4). The colloids that pass through will experience more retardation for the larger colloid and smaller grain size as demonstrated by the R values computed from moment results.

Table 3
Breakthrough experiments for bromide tracer and colloids.

Experiment		1	2	3	4
Medium	Ottawa sand	2030		mix	
Colloid	Size (μm)	0.45	3.2	0.45	3.2
Column	q (cm/min)	0.100	0.103	0.104	0.108
	ε	0.367	0.362	0.328	0.336
	L (cm)	13.28	13.1	12.4	12.5
Bromide					
Moments	$m_0=t_o$ (min)	76.9	75.7	74.5	78.2
	M_1 (min)	87.1	85.4	77.9	78.9
	R	1.01	1.04	1.04	1.02
ADE	R	1.00	1.03	1.04	1.16
	D (cm^2/min)	0.021	0.020	0.031	0.032
	r^2	0.998	0.997	0.989	0.928
PNE	R	1.01	1.04	1.03	1.03
	D (cm^2/min)	0.020	0.017	0.031	0.015
	α (1/min)	1.48×10^{-4}	7.1×10^{-4}	1.72×10^{-2}	2.51×10^{-4}
	θ_m/θ	0.994	0.980	0.989	0.984
	r^2	0.999	0.998	0.989	0.998
Colloids					
Moments	$m_0=t_o$ (min)	69.2	33.8	74.0	9.49
	M_1 (min)	90.4	86.4	80.7	86.7
	R	1.15	1.52	1.12	2.10
ADE	R	1.12	1.57	1.05	2.18
	D (cm^2/min)	0.15	0.44	0.088	0.48
	r^2	0.969	0.864	0.980	0.889
CNE	R	2.22	31.0	1.27	358
	D (cm^2/min)	0.051	0.053	0.042	2. 59
	β (1/min)	3.06×10^{-3}	5.64×10^{-4}	1.31×10^{-2}	3.74×10^{-4}
	f	0	0	1.31×10^{-2}	0.009
	r^2	0.997	0.920	0.993	0.925
PCNE	R	2.22	31.0	1.27	437
	D (cm^2/min)	0.051	0.053	0.042	0.059
	β (1/min)	3.06×10^{-3}	5.64×10^{-4}	1.31×10^{-2}	4.92×10^{-4}
	f	0.001	0.001	0.031	0.019
	α (1/min)	8.26×10^{-4}	2.88×10^{-4}	1.5×10^{-3}	6.38×10^{-3}
	θ_m/θ	0.576	0.039	0.903	0.312
	r^2	0.998	0.956	0.993	0.973

Optimizing the observations with the solution of the ADE, using D and R as optimization parameters, yields a relatively poor fit — especially in the case of the lower mass recoveries for experiments 2 and 4. Values for D are unrealistically high whereas the r^2 values suggest a poor fit (cf. Fig. 7). It should be noted again that the equilibrium model did provide a good description of the curves for the simultaneously applied bromide. Apparently additional processes affect colloid transport. First consider using the CNE model to describe the data with optimization parameters D, R (inferred from the "total" distribution coefficient K), fraction of "equilibrium" sites f, and rate parameter β. The observations are described considerably better with the CNE than the ADE, the greatest improvements occur for the 3.2-μm colloids (i.e., r^2 increased from 0.864 to 0.920 for experiment 2 and from 0.869 to 0.925 for experiment 4). The breakthrough curves predicted with these parameters describe the observations fairly well for the 0.45-μm colloids and reasonably well for the 3.2-μm colloids (Fig. 7). Including some type of nonequilibrium model seems to improve the description. Especially the large colloids are excluded from part of the aqueous phase (PNE) and experience prolonged retention (CNE). Therefore, the PCNE was also employed to describe the observations using D, R, f, β, α and θ_m/θ as optimization parameters. To minimize the number of optimization parameters, no distinction is made between f and β for the "mobile" and "immobile" region. The optimization results can be found in the last seven rows of Table 3. Application of the PCNE model leads to a slightly better description of the data than with the CNE model. The improvements are most noticeable for the 3.2-μm colloids (i.e., r^2 from 0.920 to 0.956 for experiment 2 and from 0.925 to 0.973 for experiment 4). Fig. 7 also suggests that the curves predicted with the PCNE model are more suited to describe the abrupt changes in colloid concentrations. The utility of the PCNE model will likely increase for modeling transport in natural porous media rather than in the uniform, packed sand columns where there was virtually no nonequilibrium for bromide.

4. Summary and conclusions

The advection–dispersion equation was adapted to separately account for physical and chemical nonequilibrium during transport of solutes and colloids in porous media. In the resulting physical–chemical nonequilibrium (PCNE) model the aqueous phase is partitioned into immobile and mobile regions. Based on equilibrium or nonequilibrium interaction of solutes or colloids with the solid phase, four types of solid domains may be distinguished (cf. Fig. 1). Although analytical solutions may appear to have limited applicability, there are several reasons to have analytical tools available to quantify PNCE transport. A solution for the "mobile" concentration of the PCNE was obtained with Laplace transforms (Appendix A). Expressions for other concentration types are given in Appendix B. The solution can be evaluated numerically to quantify concentration as a function of time or distance; here only breakthrough curves are considered. Furthermore, expressions for the first three time moments of the solutions are presented in Table 2. These may be used to elucidate the impact of transport parameters on the mean, variance, and skewness of breakthrough curves.

The sensitivity of the breakthrough curves to model parameters was illustrated for different types of nonequilibrium using the analytical solution for the PCNE model. The simplest cases involve the dependency of the curve on the PNE parameter θ_m/θ (Fig. 2) and the CNE parameters f_m and f_{im} in the presence of physical nonequilibrium (Fig. 3). The curves exhibit the characteristic features of earlier breakthrough and

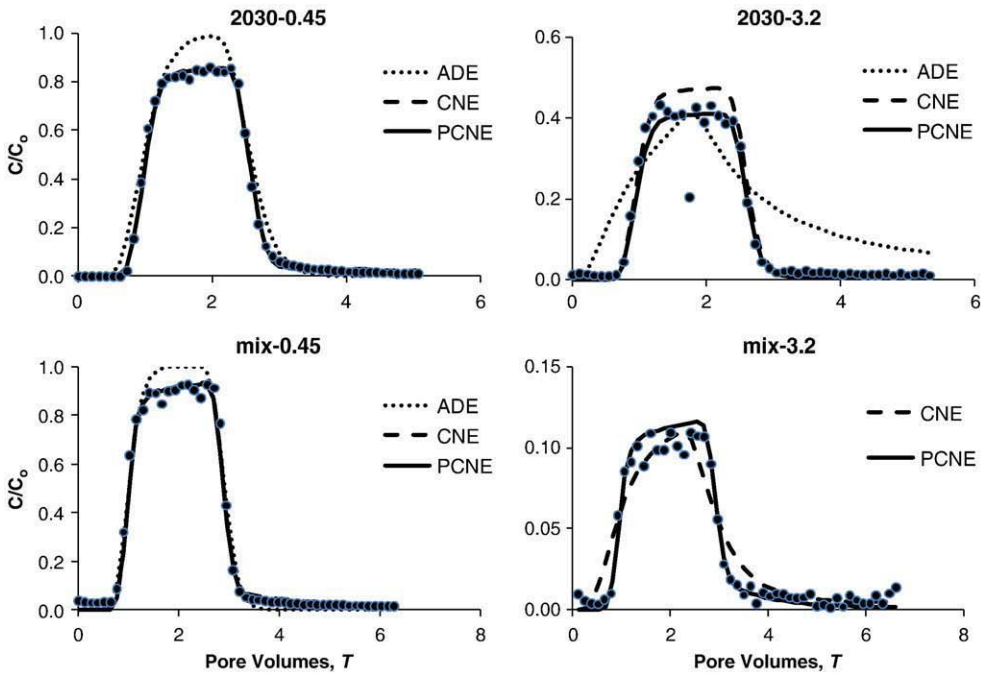

Fig. 7. Normalized colloid concentration in effluent samples (observations and optimized solution of the ADE, CNE and PCNE) as a function of normalized time for transport of smallest and largest colloid (0.45 and 3.2 μm) in two Ottawa sands with median grain sizes 710 and 240 μm (2030 and mix).

more tailing with increased nonequilibrium. However, the shape of the curves is not very sensitive to the parameter values. On the other hand, the shape of the curve will change with different combinations of the PCNE parameters α and β (Fig. 4). The additional parameters in the PCNE allow greater flexibility to generate different types of breakthrough curves. The moment results of Table 2 were used to predict contours of M_1, Var, and γ as a function of either logα and log $k_{im,a}$ (Fig. 5) or θ_{im} and log $k_{im,a}$ (Fig. 6). Both figures also illustrate the utility of having a model with independent physical and chemical nonequilibrium terms to correctly describe mean breakthrough time, variance, and skewness of colloid breakthrough curves.

Colloid transport will be affected by physical nonequilibrium because all pores are not (readily) accessible and by chemical nonequilibrium due to (different) attachment and detachment rates. These nonequilibrium phenomena are intertwined because attachment/detachment rates depend on flow regime. The PCNE model, with its ability to independently model physical and chemical nonequilibrium, was therefore applied to four colloid breakthrough experiments by Bradford et al. (2002). Breakthrough curves for the bromide tracer were described fairly well with the equilibrium ADE, use of the PNE model did not noticeably improve the optimization for these packed and uniform sands. On the other hand, the colloid breakthrough curve could not be described well using the simple ADE. Using the nonequilibrium CNE yielded a substantially better fit of the colloid data. In particular for the larger 3.2-μm colloids (experiments 2 and 4), the fit became even better when the PCNE model was employed. The need for added parameters was also illustrated by Fig. 4. There was no need for the other experiments to use the PCNE model with its additional fitting parameters. Results of the optimization algorithm showed strong correlation between PCNE parameters suggesting an excessive number of fitting parameters. It should be noted that independently quantifying physical and chemical nonequilibrium processes will become more useful for transport in natural porous media where, even for solutes such as the bromide tracer, nonequilibrium phenomena may no longer be ignored.

Acknowledgments

This research was supported by the NP206 Manure and Byproduct Utilization Project of the USDA-ARS and an interagency agreement with the EPA (IAG # DW-12-92189901-0). Although this work was funded in part by the EPA, it has not been subjected to Agency review and therefore does not necessarily reflect the views of the Agency, and no official endorsement should be inferred.

Appendix A. Solution procedure

A.1. Solution in Laplace domain

The mathematical problem given by Eqs. (10)–(12) is solved by applying a Laplace transform with respect to time with p as transformation variable. Writing the mathematical problem in terms of the transformed variables leads to:

$$p\,\overline{C}_m + p\frac{\rho_b}{\theta_m}\,\overline{S}_m + \frac{\alpha}{\theta_m}(\,\overline{C}_m - \overline{C}_{im}) = D_m\frac{d^2\,\overline{C}_m}{dz^2} - v_m\frac{d\,\overline{C}_m}{dz} \tag{A1a}$$

$$\overline{C}_{im} = \frac{\alpha\,\overline{C}_m - \rho_b p\,\overline{S}_{im}}{\theta_{im}p + \alpha} \tag{A1b}$$

$$\overline{S}_{m,1} = f_m K_m\,\overline{C}_m\,,\quad \overline{S}_{m,2} = \frac{(1-f_m)K_m}{p+\beta_m}\beta_m\,\overline{C}_m\,,\quad \overline{S}_{im,1} = f_{im}K_{im}\,\overline{C}_{im}\,,\quad \overline{S}_{im,2} = \frac{(1-f_{im})K_{im}}{p+\beta_{im}}\beta_{im}\,\overline{C}_{im} \tag{A1c, d, e, f}$$

Addition of (A1c) and (A1d), and of (A1e) and (A1f) yields

$$\overline{S}_m = f_m K_m\,\overline{C}_m + \frac{(1-f_m)K_m}{p+\beta_m}\beta_m\,\overline{C}_m\,,\quad \overline{S}_{im} = f_{im}K_{im}\,\overline{C}_{im} + \frac{(1-f_{im})K_{im}}{p+\beta_{im}}\beta_{im}\,\overline{C}_{im} \tag{A2a, b}$$

The problem is solved by using the mobile concentration as dependent variable, the other concentrations can be obtained from the solution for C_m. Substitution of (A2b) into (A1b) results in

$$\left[\frac{\alpha}{\theta_{im}} + p\left(1 + \frac{\rho_b f_{im}K_{im}}{\theta_{im}}\right) + \beta_{im}\frac{\rho_b(1-f_{im})K_{im}}{\theta_{im}}\left(1 - \frac{\beta_{im}}{p+\beta_{im}}\right)\right]\overline{C}_{im} = \frac{\alpha}{\theta_{im}}\,\overline{C}_m \tag{A3}$$

We can employ the various retardation factors defined in Table 1 for the PCNE model to establish the following relationship:

$$\overline{C}_{im} = \frac{\alpha}{\theta_{im}}\,\overline{C}_m \Big/ \left[\frac{\alpha}{\theta_{im}} + pR_{im,1} + \beta_{im}R_{im,2}\left(1 - \frac{\beta_{im}}{p+\beta_{im}}\right)\right] \tag{A4}$$

Substitute (A2a) and (A4) into (A1a) to obtain the ordinary differential equation

$$D_m \frac{d^2\,\overline{C}_m}{dz^2} - v_m \frac{d\,\overline{C}_m}{dz} - R_{m,1}\Omega(p)\,\overline{C}_m = 0 \tag{A5}$$

The auxiliary functions are as follows

$$\Omega(p) = p + a_m + b_m - \frac{\beta_m b_m}{p+\beta_m} - \frac{a_m a_{im}}{p + a_{im} + b_{im} - \beta_{im} b_{im}/(p+\beta_{im})} \tag{A6}$$

$$\Xi(p) = 1 + \frac{b_m}{p+\beta_m} + \frac{a_m[1 + b_{im}/(p+\beta_{im})]}{p + a_{im} + b_{im} - \beta_{im} b_{im}/(p+\beta_{im})} \tag{A7}$$

with variables a and b as defined in Table 1. The transformed boundary conditions are:

$$\overline{C}_m(0,p) = \overline{C}_o(p)\,, \quad \overline{C}_m(\infty,p) = 0 \tag{A8a, b}$$

The solution of the (transformed) mobile concentration is

$$\overline{C}_m(z,p) = \overline{C}_o exp\left(\frac{v_m z}{2D_m} - \frac{z}{\sqrt{D_m/R_{m,1}}}\sqrt{\Omega(p) + \frac{v_m^2}{4R_{m,1}D_m}}\right) \tag{A9}$$

A.2. Inversion procedure

Transformation to the temporal domain is somewhat cumbersome and is based on the iterated Laplace transform (Sneddon, 1995). Inversion of (A9) involves sequential application of the shifting and convolution theorems. The following Laplace transformation pairs were used:

$$L^{-1}\{exp(-k\sqrt{p})\} = \frac{k}{\sqrt{4\pi t^3}} exp\left(-\frac{k^2}{4t}\right) \tag{A10}$$

$$L^{-1}\left\{exp\left(\frac{k}{p+a}\right)\right\} = exp(-at)\left[\delta(t) + \sqrt{\frac{k}{t}} I_1(\sqrt{4kt})\right] \tag{A11}$$

where L^{-1} denotes inversion, $\delta(t)$ is the Dirac delta function, I_1 is the modified first-order Bessel function, and a and k are arbitrary constants.

The shifting theorem is used to invert the first Laplace variable of the auxiliary function Ω to obtain:

$$C_m(z,t) = \int_0^t C_o(t-\tau)\int_0^\tau L^{-1}_{\tau-\eta}\left\{exp\left(\frac{v_m z}{2D_m} - \frac{z\sqrt{p}}{\sqrt{D_m/R_{m,1}}}\right)\right\} \times L^{-1}_{\eta}\left\{exp\left[-\left(\frac{v_m^2}{4R_m D_m} + a_m + b_m - \frac{\beta_m b_m}{p+\beta_m} - \frac{a_m a_{im}}{p + a_{im} + b_{im} - \beta_{im} b_{im}/(p+\beta_{im})}\right)(\tau-\eta)\right]\right\} d\eta\, d\tau \tag{A12}$$

The subscript of the Laplace operator denotes the variable to which the Laplace variable is inverted to. Next (A10) is used and the remaining exponential functions with Laplace variables are written as a convolution integral:

$$C_m(z,t) = \int_0^t \int_0^\tau \frac{z C_o(t-\tau)\sqrt{R_{m1}}}{\sqrt{4\pi D_m(\tau-\eta)^3}} exp\left[\frac{v_m z}{2D_m} - \frac{R_{m1} z^2}{4D_m(\tau-\eta)} - \left(\frac{v_m^2}{4D_m R_{m,1}} + a_m + b_m\right)(\tau-\eta)\right] \times \int_0^\eta L^{-1}_{\eta-\sigma}\left\{exp\left(\frac{\beta_m b_m(\tau-\eta)}{p+\beta_m}\right)\right\} L^{-1}_{\sigma}\left\{exp\left(\frac{a_m a_{im}(\tau-\eta)}{p + a_{im} + b_{im} - \beta_{im} b_{im}/(p+\beta_{im})}\right)\right\} d\sigma\, d\eta\, d\tau \tag{A13}$$

The first inversion is done according to (A11) while the shifting and convolution theorems are, again, used for the second inversion:

$$C_m(z,t) = \int_0^t \int_0^\tau \frac{zC_o(t-\tau)\sqrt{R_{m,1}}}{\sqrt{4\pi D_m(\tau-\eta)^3}} exp\left(-(a_m + b_m)(\tau-\eta) - \frac{[R_{m,1}z - v_m(\tau-\eta)]^2}{4D_m R_{m,1}(\tau-\eta)}\right) \int_0^\eta exp[-\beta_m(\eta-\sigma)] \tag{A14}$$
$$\times \left\{\delta(\eta-\sigma) + \sqrt{\frac{\beta_m b_m(\tau-\eta)}{\eta-\sigma}} I_1\left[\sqrt{4\beta_m b_m(\tau-\eta)(\eta-\sigma)}\right]\right\}$$
$$\times \int_0^\sigma L_k^{-1}\left\{exp\left(\frac{\beta_{im} b_{im}(\sigma-\kappa)}{p+\beta_{im}}\right)\right\} L_{\sigma-\kappa}^{-1}\left\{exp\left(\frac{a_m a_{im}(\tau-\eta)}{p + a_{im} + b_{im}}\right)\right\} d\kappa d\sigma d\eta d\tau$$

Upon carrying out the remaining inversions, the solution may be written with the help of the auxiliary functions given by Eq. (14) as:

$$C_m(z,t) = \int_0^t C_o(t-\tau) \int_0^\tau h(z,\tau,\eta) \int_0^\eta \{\delta(\eta-\sigma) exp[-\beta_m(\eta-\sigma)] + g_m(\tau,\eta,\sigma)\} \tag{A15}$$
$$\times \int_0^\sigma \{\delta(\kappa) exp(-\beta_{im}\kappa) + g_{im}(\sigma,\kappa,0)\} \{\delta(\sigma-\kappa) exp[-(a_{im} + b_{im})(\sigma-\kappa)] + f(\tau,\eta,\sigma,\kappa)\} d\kappa d\sigma d\eta d\tau$$

The solution given by Eq. (13) is obtained after evaluating all Dirac delta functions. Integrals are evaluated numerically using Gauss–Chebyshev quadrature (Press et al., 2007).

Appendix B. Other aqueous and solid phase concentrations for PCNE model

The immobile concentration is obtained according to (cf. Eq. (A4)):

$$\overline{C}_{im} = \frac{a_{im}\,\overline{C}_m}{p + a_{im} + b_{im} - \beta_{im} b_{im} / (p + \beta_{im})} \tag{B1}$$

Inversion is accomplished with the results for the mobile concentrations and a table of Laplace transforms or Mathematica, the result may be written for a constant influent concentration as:

$$C_{im}(z,t) = \int_0^t C_o \left\{1 + \frac{w_4 - w_3}{2w_3} exp\left[-(w_2 - w_3)\frac{t-\tau}{2}\right] - \frac{w_4 + w_3}{2w_3} exp\left[-(w_2 + w_3)\frac{t-\tau}{2}\right]\right\} \tag{B2}$$
$$\times \left\{h(z,\tau,0) + \int_0^\tau h(z,\tau,\eta)\left[f(\tau,\eta,\eta,0) + g_m(\tau,\eta,0) + \int_0^\eta g_{im}(\eta,\sigma,0) f(\tau,\eta,\eta,\sigma)\right.\right.$$
$$\left.\left. + g_m(\tau,\eta,\sigma)\left(f(\tau,\eta,\sigma,0) + \int_0^\sigma g_{im}(\sigma,\kappa,0) f(\tau,\eta,\sigma,\kappa) d\kappa\right) d\sigma\right] d\eta\right\} d\tau$$
$$\text{with: } w_2 = a_{im} + b_{im} + \beta_{im}, w_3 = \sqrt{w_2^2 - 4a_{im}\beta_{im}}\ ,\ w_4 = a_{im} - b_{im} - \beta_{im}$$

In case of equilibrium partitioning, the concentrations for the solid phase follow directly from the mobile and immobile regions:

$$S_{m,1} = K_m f_m C_m\ ,\ S_{im,1} = K_{im} f_{im} C_{im} \tag{B3a, b}$$

The concentrations for nonequilibrium partitioning are obtained by inverting Eqs. (A1d,f):

$$S_{m,2}(z,t) = \int_0^t C_o(1-f_m) k_m \{1 - exp[-\beta_m(t-\tau)]\} \left\{h(z,\tau,0) + \int_0^\tau h(z,\tau,\eta)\left[f(\tau,\eta,\eta,0) + g_m(\tau,\eta,0)\right.\right. \tag{B4}$$
$$\left.\left. + \int_0^\eta g_{im}(\eta,\sigma,0) f(\tau,\eta,\eta,\sigma) + g_m(\tau,\eta,\sigma)\left(f(\tau,\eta,\sigma,0) + \int_0^\sigma g_{im}(\sigma,\kappa,0) f(\tau,\eta,\sigma,\kappa) d\kappa\right) d\sigma\right] d\eta\right\} d\tau$$

$$S_{im,2}(z,t) = \int_0^t (1-f_{im})k_{im}C_o\left\{1 + \frac{2a_{im}\beta_{im}}{w_3(w_2+w_3)}exp\left[-(w_2+w_3)\frac{t-\tau}{2}\right] - \frac{2a_{im}\beta_{im}}{w_3(w_2-w_3)}exp\left[-(w_2-w_3)\frac{t-\tau}{2}\right]\right\} \quad \text{(B5)}$$
$$\times\left\{h(z,\tau,0) + \int_0^{\tau} h(z,\tau,\eta)\left[f(\tau,\eta,\eta,0) + g_m(\tau,\eta,0) + \int_0^{\eta} g_{im}(\eta,\sigma,0)f(\tau,\eta,\eta,\sigma)\right.\right.$$
$$\left.\left. + g_m(\tau,\eta,\sigma)\left(f(\tau,\eta,\sigma,0) + \int_0^{\sigma} g_{im}(\sigma,\kappa,0)f(\tau,\eta,\sigma,\kappa)d\kappa\right)d\sigma\right]d\eta\right\}d\tau$$

References

Bradford, S.A., Torkzaban, S., 2008. Colloid transport and retention in unsaturated porous media: a review of interface, collector, and pore scale processes and models. Vadose Zone J. 7, 667–681.

Bradford, S.A., Yates, S.R., Bettahar, M., Simunek, J., 2002. Physical factors affecting the transport and fate of colloids in saturated porous media. Water Resour. Res. 38 (12), 1327. doi:10.1029/2002WR001340.

Bradford, S.A., Simunek, J., Bettahar, M., van Genuchten, M.Th., Yates, S.R., 2006. Significance of straining in colloid deposition: evidence and implications. Water Resour. Res. 42, W12S15. doi:10.1029/2005WR004791.

Bradford, S.A., Torkzaban, S., Walker, S.L., 2007. Coupling of physical and chemical mechanisms of colloid straining in saturated porous media. Water Res. 41, 3012–3024.

Brusseau, M.L., Jessup, R.E., Rao, P.S.C., 1989. Modeling the transport of solutes influenced by multiprocess nonequilibrium. Water Resour. Res. 25, 1971–1988.

Brusseau, M.L., Jessup, R.E., Rao, P.S.C., 1992. Modeling solute transport influenced by multiprocess nonequilibrium and transformation reactions. Water Resour. Res. 28, 175–182.

Coats, K.H., Smith, B.D., 1964. Dead-end pore volume and dispersion in porous media. Soc. Pet. Eng. J. 4, 73–84.

de Rooij, G.H., 2000. Modeling fingered flow of water in soils owing to wetting front instability: a review. J. Hydrol. 231–232, 277–294.

Johnson, W.P., Li, X., Yal, G., 2007. Colloid retention in porous media: mechanistic confirmation of wedging and retention in zones of flow stagnation. Environ. Sci. Technol. 41, 1279–1287.

Leij, F.J., Toride, N., 1998. Analytical solutions for nonequilibrium transport. In: Selim, H.M., Ma, L. (Eds.), Physical Nonequilibrium in Soils: Modeling and Applications. Ann Arbor Press, Chelsea, MI, pp. 117–156.

Neville, C.J., Ibaraki, M., Sudicky, E.A., 2000. Solute transport with multi-process nonequilibrium: a semi-analytical solution approach. J. Contam. Hydrol. 44, 141–159.

Powers, S.E., Loureiro, C.O., Abriola, L.M., Weber, W.J., 1991. Theoretical study of the significance of nonequilibrium dissolution of nonaqueous phase liquid in subsurface systems. Water Resour. Res. 27, 463–477.

Press, W.H., Teukolsky, S.A., Vetterling, W.T., Flannery, B.P., 2007. Numerical Recipes (3rd Edition): The Art of Scientific Computing. Cambridge Univ. Press, Cambridge, UK.

Ritsema, C.J., Dekker, L.W., Hendrickx, J.H.M., Hamminga, W., 1993. Preferential flow mechanism in a water repellent soil. Water Resour. Res. 29, 2183–2193.

Sardin, M., Schweich, D., Leij, F.J., van Genuchten, M.Th., 1991. Modeling the nonequilibrium transport of linearly interacting solutes in porous media: a review. Water Resour. Res. 27, 2287–2307.

Selim, H.M., Ma, L. (Eds.), 1998. Physical Nonequilibrium in Soils: Modeling and Application. Ann Arbor Press, Inc., Chelsea, MI.

Selim, H.M., Ma, L., Zhu, H., 1999. Predicting solute transport in soils: second-order two-site models. Soil Sci. Soc. Am. J. 63, 768–777.

Sneddon, I., 1995. Fourier Transforms. Dover, New York.

Sparks, D.L., 1989. Kinetics of Soil Chemical Processes. Academic Press, San Diego.

Toride, N., Leij, F.J., van Genuchten, M.Th., 1993. A comprehensive set of analytical solutions for nonequilibrium solute transport with first-order decay and zero-order production. Water Resour. Res. 29, 2167–2182.

Torkzaban, S., Bradford, S.A., Walker, S.L., 2007. Resolving the coupled effects of hydrodynamics and DLVO forces on colloid attachment to porous media. Langmuir 23, 9652–9660.

Torkzaban, S., Tazehkand, S.S., Walker, S.L., Bradford, S.A., 2008. Transport and fate of bacteria in porous media: coupled effects of chemical conditions and pore space geometry. Water Resour. Res. 44, W04403. doi:10.1029/2007WR006541.

Valocchi, A.J., 1985. Validity of the local equilibrium assumption for modeling sorbing solute transport through homogeneous soils. Water Resour. Res. 21, 808–820.

van Genuchten, M.Th., Wierenga, P.J., 1976. Mass transfer studies in sorbing porous media: I. Analytical solutions. Soil Sci. Soc. Am. J. 40, 473–480.

Wagenet, R.J., Chen, W., 1998. Coupling sorption rate heterogeneity and physical nonequilibrium in soils. In: Selim, H.M., Ma, L. (Eds.), Physical Nonequilibrium in Soils: Modeling and Applications. Ann Arbor Press, Chelsea, MI, pp. 117–156.

Wang, Z., Jury, W.A., Tuli, A., Kilm, D.-J., 2004. Unstable flow during redistribution: controlling factors and practical implications. Vadose Zone J. 3, 549–559.